DIGITAL LIBRARY

dspace.vutbr.cz

Insight into the response time of fail-safe magnetorheological damper

JENIŠ, F.; KUBÍK, M.; MACHÁČEK, O.; ŠEBESTA, K.; STRECKER, Z.

Smart Materials and Structures
2021, vol. 30, iss. 1, pp. 1-13

ISSN: 1361-665X

DOI: http://dx.doi.org/10.1088/1361-665X/abc26f

Accepted manuscript

Citation:

JENIŠ, F.; KUBÍK, M.; MACHÁČEK, O.; ŠEBESTA, K.; STRECKER, Z. (2021). Insight into the response time of fail-safe magnetorheological damper. *Smart Materials and Structures*, 30(1), 1–13. https://doi.org/10.1088/1361-665X/abc26f

This is the Accepted Manuscript version of an article accepted for publication in Smart Materials and Structures .IOP Publishing Ltd is not responsible for any errors or omissions in this version of the manuscript or any version derived from it. The Version of Record is available online at 10.1088/1361-665X/abc26f.

Insight into the response time of fail-safe magnetorheological damper

Jeniš F.[1], Kubík M., Macháček O., Šebesta K. and Strecker Z.

[1] Brno University of Technology, Brno, Czechia

E-mail: filip.jenis@vutbr.cz

Received xxxxxx
Accepted for publication xxxxxx
Published xxxxxx

Abstract

The significant problem of magnetorheological (MR) dampers is their poor fail-safe ability. In the case of power supply failure, the damper remains in a low damping state which is dangerous for several technical applications. This can be solved by accommodating a permanent magnet to the magnetic circuit of the damper. Currently, the MR dampers are used in progressive semiactive (S/A) control of suspension systems. The dynamics (force response time) of the damper is an important parameter that affects the performance of semiactive control. The main goal of this paper is to introduce the dynamic behavior of MR damper with a permanent magnet. The damper design with the permanent magnet in the magnetic circuit, transient magnetic simulation including magnetic hysteresis and eddy currents, and experiments are presented. The magnetic field response time and MR damper force response time are measured and also determined from magnetic simulation. The permanent magnet significantly influences the MR damper dynamics. The decrease of the damping force from a fail-safe state – medium damping to off-state – low damping is significantly faster (2 ms, -1A) than the increase to on-state – high damping (12 ms, 1A). The exact value is depending on the electric current magnitude and piston velocity. The damper achieved fail-safe damping force approximately 1/3 of the maximum damping force. The exact value of the fail-safe force is magnetization history-dependent. The maximum dynamic force range is 8.5 which is comparable with the common design of MR damper.

Keywords: magnetorheological valve, MR damper, response time, permanent magnet, fail-safe, transient response, damper dynamics

1. Introduction

The main aim of the car suspension system is to provide maximum ride comfort and handling stability. Three types of suspension systems, namely, passive, semiactive (S/A), and active are commonly used. The passive suspension system can´t effectively mitigate vehicle vibration on passengers because the damping cannot be changed according to the actual situation. In the case of the active suspension system, linear electric motor or electric pump [1], are used to control vehicle body motion over a wide frequency range. The main disadvantages of the active system are their high energy consumption, high cost, or stability problem. The S/A suspension systems offer a compromise between suspension system performance and cost. The S/A system requires low energy source and provide significantly higher ride comfort and handling stability than passive systems. Since the 1970s [2], the control strategy and suitable dampers have been widely studied for different technical applications.

The performance of S/A control of the suspension system is significantly influenced by the dynamic behavior of the damper. The response time of the damper on the control signal is a key factor [3]. A rapid increase or decrease of damping

 © xxxx IOP Publishing Ltd

level (short response time) on the control signal is desired for all real-time S/A control applications [4]. Giua et al. [5] simulated influence of damper response time on to S/A control performance. The damper with response time 7 ms exhibits better results in terms of performance S/A suspension system than damping element with response time 30 ms. Similar conclusions can be found in publications [3,6]. Suitable dampers for real-time S/A control are the hydraulic solenoid valve damper and the magnetorheological (MR) damper.

A solenoid valve damper varies the size of an orifice by an electromagnetic coil, which can give continuously variable damping characteristics. This technology offers several companies (Sachs ZF, Tenneco, etc.) under various trade names such as CDC, DCC, etc. This damper can be designed with fail-safe behaviour, ie. the maximum damping force is generated in a damper with no electric current. Qin [7] measured the dynamic behaviour of the CDC solenoid damper. The response time for the force rise (soft -> hard) was in the range 16 ms to 24 ms; the response time for the force drop (hard -> soft) was in the range 7 ms to 15 ms. The dynamic behavior of the solenoid valve damper has also been addressed in [8].

The magnetorheological (MR) damper utilizing magnetorheological MR fluid which, when subjected to magnetic stimuli generates yield stress thus increasing the apparent viscosity of the fluid [9]. MR fluid is a suspension of microsized ferromagnetic particles which are dispersed in the carrier fluid. These particles are chained in the direction of the magnetic field and cause a significant increase in the apparent viscosity and damping forces. The sedimentation stability of MR fluid (particles) is intensively addressed in [10–13]. In papers can be found several MR damper designs that differ in the number of coils [14–16], the arrangement of the magnetic circuit [17], the number of gaps [18,19], etc. If the power supply of the coil is interrupted, the damper will stay at the minimum damping level. This is a significant problem for a wide range of MR damper applications (aerospace, rail, automotive, etc.). A suitable solution is to use a permanent magnet into the MR damper magnetic circuit. The permanent magnet creates a magnetic flux in the magnetic circuit, which ensures damping during a power supply failure – fail-safe state. In some designs, the permanent magnet is placed under the inner edge of the electromagnetic coil [20–23] or next to the electromagnetic coil on the edge of the piston gap [24,25]. The damping level with no electric current and with permanent magnet usually achieved one-third of the maximum force. Also, a low–coercivity magnet accommodated in the magnetic circuit (e.g. Alnico, made of Aluminium – Nickel - Cobalt) can provide the MR damper with non–minimal damping forces without external power supply as mentioned in [24]. However, using a so-called switchable magnet does not ensure a full fail-safe ability of MR damper due to the possibility of magnet demagnetization.

The dynamic behavior of MR dampers dealt with only a handful of authors. Koo et al. [4] experimentally determined the response time of a commercially available Lord Corporation's Motion Master® Ride Management System at approximately 17 ms (lowest measured value). However, the response time of damper is strongly dependent on the magnitude of the applied electric current and the piston velocity. Takesue et al. [26] presented the design of the MR clutch where they improved the dynamic behavior of this actuator by reduction of eddy current in the magnetic circuit. The same aim had Strecker [27] and Kubík [16] who published the design of MR damper with a short response time where the ferrite material of the magnetic circuit was used. Strecker [17] published MR damper with a magnetic circuit manufactured by 3D metal printing, which allowed the MR damper design with a response time of 1.68 ms and a high dynamic range. This method is based on the design of the special shape of the magnetic circuit contributing to the reduction of eddy current. The effect of eddy currents on MR damper dynamics can be also reduced using a magnetic circuit made by laminated sheets [15,28]. Sahin [29] et al. compared two MR valves with similar material and different geometry. Sahin et al. showed that the response time of the MR damper is also dependent on the geometry of the MR valve. The dynamic behavior of MR damper with a permanent magnet was examined only by Lee et. al [32]. The damping force of this damper is realized by the variation of the magnetization area (position-dependent damper), not by the electromagnetic coil.

The *main aim* of this paper is to introduce the *dynamic behavior of fail-safe MR damper with a permanent magnet.* The response time of the magnetic field and force on the step the control signal are determined experimentally and using the magnetic models.

2. Materials and methods

2.1 MR damper response time

The dynamic behavior of MR damper is usually assumed as a first-order system, where the response time is determined at 63.2% of steady-state force value [9,16,27]. However, in many publications, the response time of MR damper is described as 90 % [30,31] or 95 % [4,17] of the steady-state force value. The criterion of 90 % is frequently used for the description of the dynamic behavior of actuators in industrial applications [32]. Response time (τ) of the system indirectly implies cut-off frequency ($f = \frac{1}{2\pi\tau}$) which is connected with the controllable frequency range of the damper [33]. The primary response time τ_{63}, τ_{36} (63.2 % for the rise and 36.8 % for a drop of steady-state value) and secondary response time τ_{90}, τ_{10} (90 % for the rise and 10 % for a drop of steady-state value) on step electric current drop and rise will be determined from measured and simulated data in this paper, see **Figure 1**.

The measured and simulated data were normalized by the non-dimensional function N_o. A detailed description of this method in paper [32].

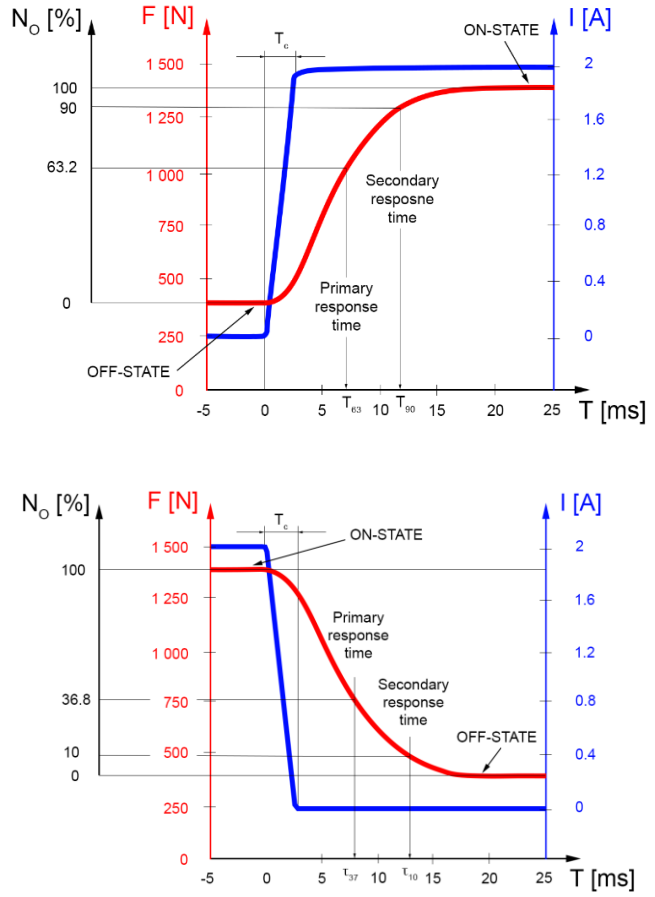

Figure 1 *Definition of the response time of MR damper*

2.2 Design of MR damper with permanent magnet

The presented MR damper is a monotube design, where the high-pressure gas (6) is separated from the MR fluid (5) by a floating piston (2), see **Figure** 2.

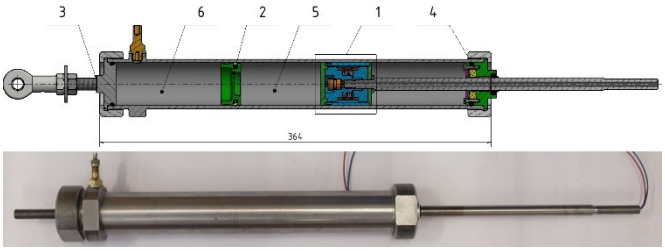

***Figure** 2 Design of MR damper with permanent magnet*

The piston rod was sealed by a piston rod seal from H-PU material and guided by bearing (4). The most important part of the damper is a piston unit (1). The damper was filled by 200 ml of MRF Lord MRF 132-DG and pressurized by 30 bar. The piston unit consists of a core (1, 2), sleeve (3), plates (4), piston rod (5), permanent magnet (6), and an electromagnetic coil (7). The important dimensions are shown in **Figure 3**.

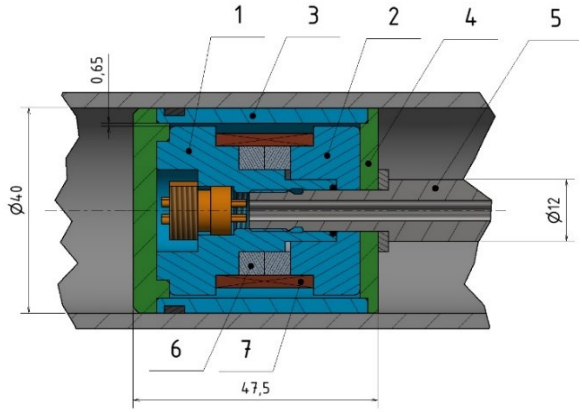

Figure 3 *The detail of MR valve with permanent magnet*

The wire of the electromagnetic coil was connected to the connector integrated into the piston rod. The magnetic circuit (1, 2, 3) was made of cutting steel (11SMn30 with a carbon content of less than 1%). Two neodymium permanent magnets in the form of a ring 25x16x5 mm, class N42 was used. These magnets have been selected because they were up for sale. The maximum operating temperature is 80 °C.

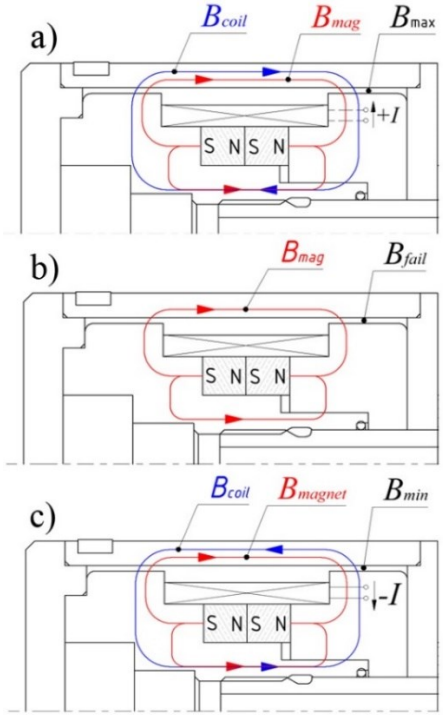

Figure 4 *The main principle of MR valve function with permanent magnet; a) current +I, b) no current, c) –I current*

An electromagnetic coil was winded by 190 turns of copper wire with a diameter of 0.5 mm. **Figure 4** shows the main principle function idea of the damper with the magnet. In the case of the positive polarity of electric current *+I*, the magnetic flux density in the gap is $B_{max} = B_{mag} + B_{coil}$. In the

case of the negative polarity of electric current *-I*, the magnetic flux density in the gap is $B_{min} = B_{mag} - B_{coil}$.

2.3 Magnetic model

The FE magnetic model is necessary for the calculation of magnetic circuit properties including significant non-linearities (magnetization curve, magnetic hysteresis, etc.). The analytical approach is considerably inaccurate due to the model complexity. The Ansys Electronics Desktop 2018 with co-simulation of Ansys Twin Builder 2018 was used for the presented models. We assumed the magnetorheological valve in the damper as asymmetric around the centerline Z in a cylindrical coordinate system. The simplified geometry of the MR valve for magnetic simulation is shown in **Figure 5**.

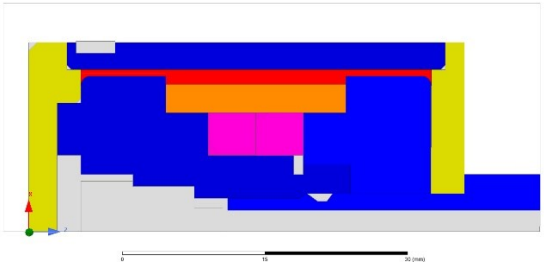

Figure 5 *Simplified geometry of MR valve for the magnetic model; steel 11SMn30 (blue), MR fluid or Air (red), bronze (yellow), NdFe42 magnet (green), copper (orange) and air surrounding (white).*

The magnetic circuit (**Figure 3** 1, 2, 3) was made of cutting steel 11SMn30. The virgin and hysteresis magnetization curve was experimentally determined for sample of this steel by system Remagraph C-500.Measured data is shown in **Figure 6**. The coercivity and remanence were determined from the measured hysteresis loop: H_c = 427 A/m and B_r = 1.05 T.

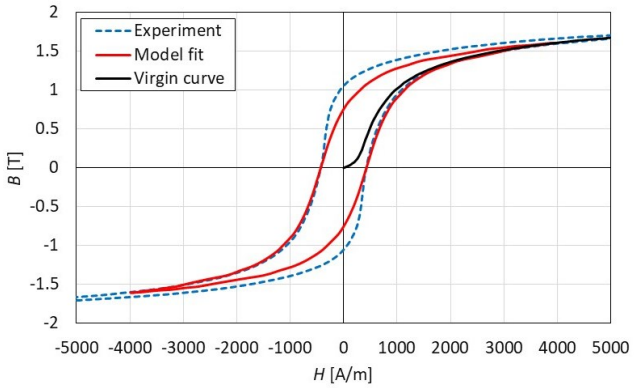

Figure 6 *The virgin (black) and hysteresis magnetization curve for steel 11SMn30; experiment (blue), model fit on experimental data (red)*

The electric bulk conductivity σ = 5.8 MS/m was used. The lids were made of bronze with relative permeability $\mu_r = 1$ and electric bulk conductivity σ =10 MS/m. The MRF 132-DG was used for models. The magnetic hysteresis of MR fluid was neglected. We applied the vector hysteresis modeling feature available in system Ansys on the electromagnetic model of the MR valve. A more detailed description of this model is in the publication [9]. The curve fit to the experimental hysteresis data for the steel 11SMn30 was created by Ansys software, see **Figure 6**. The agreement is sufficient except for low magnetic field strength. The NdFe42 permanent magnet was used in the model, see the magnetization curve from magnet manufacture in **Figure 7**. The exact geometry and magnet type were selected for availability on the market.

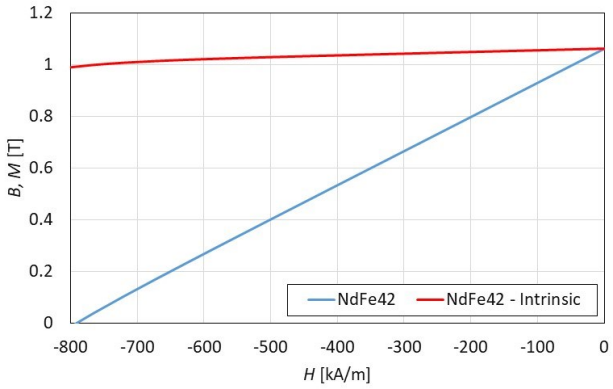

Figure 7 *Magnetisation curve of NdFe42 permanent magnet*

The magnetic model was coupled to the external electric circuit revealed in **Figure 8**. The lumped electric circuit is composed of an ideal electric current source (control input), resistor (with the resistance of coil winding), and MR valve object (non-linear inductor).

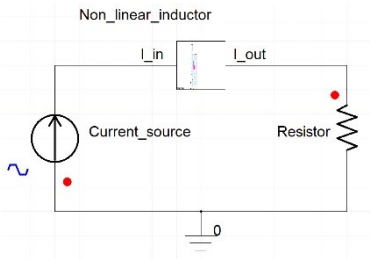

Figure 8 *Lumped electric circuit (an external electric circuit)*

The proposed magnetic model was used in two cases with different time scales to determine the quasi-static (2.2.1) and transient (2.2.2) behavior of the magnetic circuit.

2.3.1 Quasi-static magnetic model

This model was used to determine the hysteresis behavior of a magnetic circuit in two configurations: with air in the gap and with MRF in the gap. The effect of eddy currents was neglected due to slow changes in electric current. The setting of this model was used in these configurations:

a) magnetic circuit with the electromagnetic coil (air in the gap; results in **Figure 11**),

b) magnetic circuit with electromagnetic coil and magnet (air and MRF in the gap; results in **Figure 12** and **Figure 13**).

This model allows us to design a proper geometry of the magnetic circuit to maximize fail-safe magnetic flux and minimize the effect of the magnet in the gap in off-state.

2.3.2 Transient magnetic model

This model calculates the magnetic induction (flux density) course in the gap on step current input. The response times are determined from these data. The final value of the electric current (T_c) was reached at $T_c = 0.2\ ms$. Therefore, it is assumed that it is the step control signal in the simulation. This value has been selected due to previous experimental experiences. The waveforms of electric current were different for different settings of this simulation. The constant simulation time step was set at 0.2 ms. The mesh was generated with refinement on the edges of the magnetic circuit due to the rapid creation of eddy current on these areas. The setting of this model was used in these configurations:

a) magnetic circuit with electromagnetic coil and MRF in the gap (results in **Figure 16**),
b) magnetic circuit with an electromagnetic coil, permanent magnet and air in the gap (results in **Figure 15**),
c) magnetic circuit with an electromagnetic coil, permanent magnet, and MRF in the gap (results in **Figure 17**).

2.4 Measurement setup of B-I map and magnetic circuit dynamics with the air gap

This measurement was carried out for verification of the modeling method. Measuring magnetic flux density with Hall probe can only be measured material in the gap with relative permeability $\mu_r = 1$ (air). It can be assumed, that the magnetic model verified with air in the gap will be valid for MR fluid in the gap as well. Four types of measurement with the almost identical configuration of measuring setup were carried out: (a) quasi-static properties of the magnetic circuit with permanent magnet and electromagnetic coil; (b) quasi-static properties of the magnetic circuit with electromagnetic coil; (c) response time of magnetic flux density on the electric current step in configuration with permanent magnet and electromagnetic coil; and (d) response time of magnetic flux density on the electric current step in configuration with an electromagnetic coil. For the response time measurement, the own patented current controller working with the overvoltage method was used [27]. The controller is supplied by laboratory supply and the input signal was generated from the Arduino control board. The increase in current took *0.2 ms*. The experimental setup diagram can be seen in **Figure 9**. The magnetic flux density was measured by a teslameter (F.W. Bell 5180) with an ultra-thin transverse probe (STB1X-0201). The course of electric current was measured by current clamp Fluke i30s. These two signal was measured with a sampling frequency of 200 kHz by font-end Dewetron USB-50. The measured data was processed by the software DeweSoft.

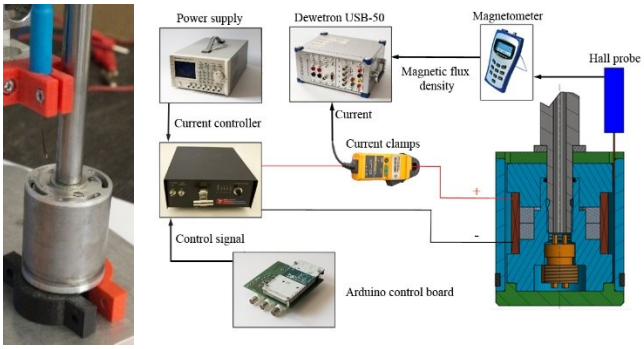

Figure 9 *Experimental setup for magnetic behaviour measurement*

2.5 Measurement setup of F-v-I map

The measurement of the F-v-I (force-velocity-electric current) map was performed on the hydraulic pulsator Inova, see **Figure 10**. Logarithmic sweep with a constant amplitude of 25 mm was used as an excitation signal in the frequency range 0.05 – 1.91 Hz, therefore, the velocity was increasing during the test. The maximum velocity was 0.2 m/s. The load gauge 1730 ACK-50 kN was used for the force measurement, the position of piston-rod was measured by resistance sensor VLP15$A150, the current was calculated from the voltage drop on 0.1 Ω power shunt, and the temperature was measured by sensor PT35. The presented temperature was measured on the hydraulic tube surface of the MR damper in the range 37°C– 43°C. These signals were recorded with a sampling frequency of 50 kHz by analyzer Dewe-800.

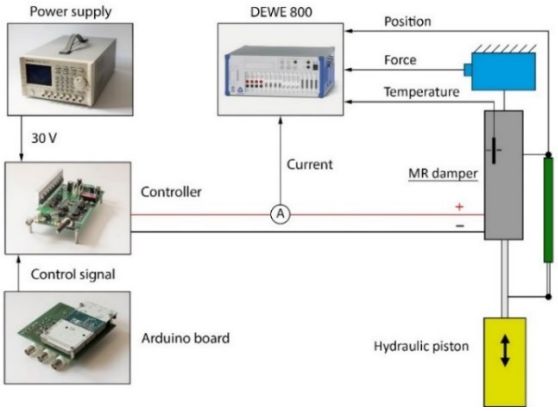

Figure 10 *Experimental setup for F-v-I measurement*

On the control board Arduino was set constant electric current 1A, 2A, 0A(+) and with opposite polarity -1A, -2A, 0A(-). The piston velocity was calculated by derivation of the piston position. The F-v-I map was calculated from measured data

choosing the points with zero acceleration (center of the stroke).

2.6 Measurement setup of MR damper dynamics (force response time)

For the force response time measurement was used load gauge HBM U2AD1/2. The configuration of the measurement was the same as in chapter 2.4. The control signal was generated by the Inova control computer. This signal was input into the Arduino board and then to the current controller. The electric current was switched always after two strokes of the MR damper in the middle of the stroke. Measurement of transient response was carried out for piston velocity 0.2 m/s and electric currents 0.5A, 1A, 1.5A, 2A, and for the same values with opposite polarity. Measurement of the rise and drop of the force was performed 5x and the response time was determined as the average of these values for each electric current.

3. Results and discussion

3.1 Quasi-static magnetic behavior

This section aims to compare the magnetic model with an experiment for configuration with and without a permanent magnet. **Figure 11** shows the comparison between the magnetic model (full line) and experiment (dotted line) for configuration without magnet and air in the gap. The magnetic circuit exhibits a remanent flux density of 22 mT in the gap. The agreement between model and experiment is very good. The maximum error is 15 % at zero electric currents. This difference is probably given by an inaccurate fit of the hysteresis magnetization curve, see **Figure 6**.

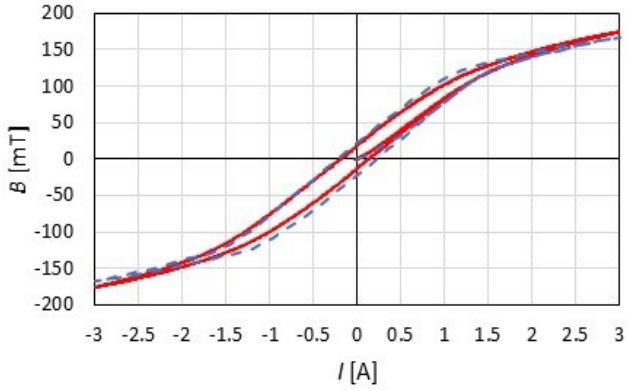

Figure 11 *Comparison of the magnetic model (full line) and experiment (dotted line) for configuration without magnet and with air in the gap*

Figure 12 shows the comparison between the magnetic model (full line) and experiment (dotted line) for configuration with the magnet and air in the gap. Remanent flux density 101 mT and 90 mT were measured in the gap at zero electric currents. The accuracy of the model is good except for the low electric current.

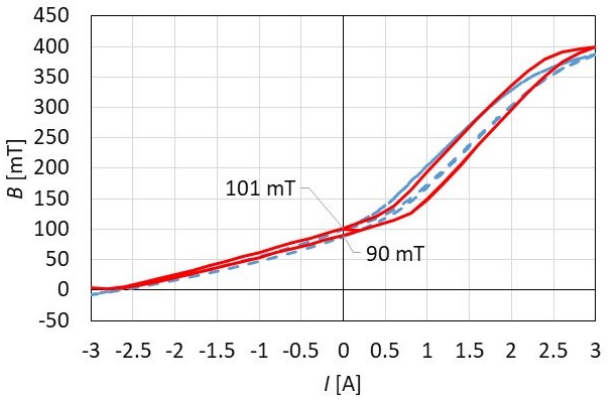

Figure 12 *Comparison of the magnetic model (full line) and experiment (dotted line) for configuration with magnet and air in the gap*

The fail-safe magnetic flux density in the gap creates roughly one-fourth of the maximum. This experimentally verified model was used to determine magnetic behavior with MRF in the gap, see **Figure 13**. The fail-safe magnetic flux density (B_{fail}) in the gap creates roughly one-third of the maximum flux density. However, the B_{fail} value is a magnetization history-dependent.

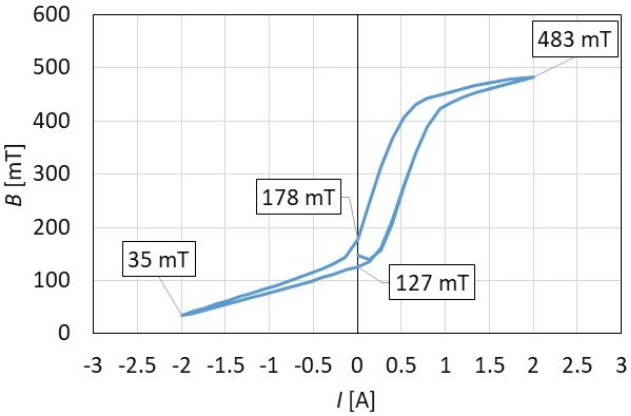

Figure 13 *Hysteresis B-I curve of MR damper with MRF in the gap and permanent magnet*

3.2 Magnetic circuit dynamics

Magnetic flux response on a different input of electric current and a different configuration of magnetic circuit were compared for the magnetic model and experiment.

3.2.1 Magnetic circuit with air in the gap (magnet and coil)

This section is important for experimental verification of the transient magnetic model. **Figure 14** shows the course of magnetic flux density determined from the magnetic model (red) and experiment (blue) for the electric current step from *0A* to *-1A*. Measured data were normalized in the bottom

diagram.

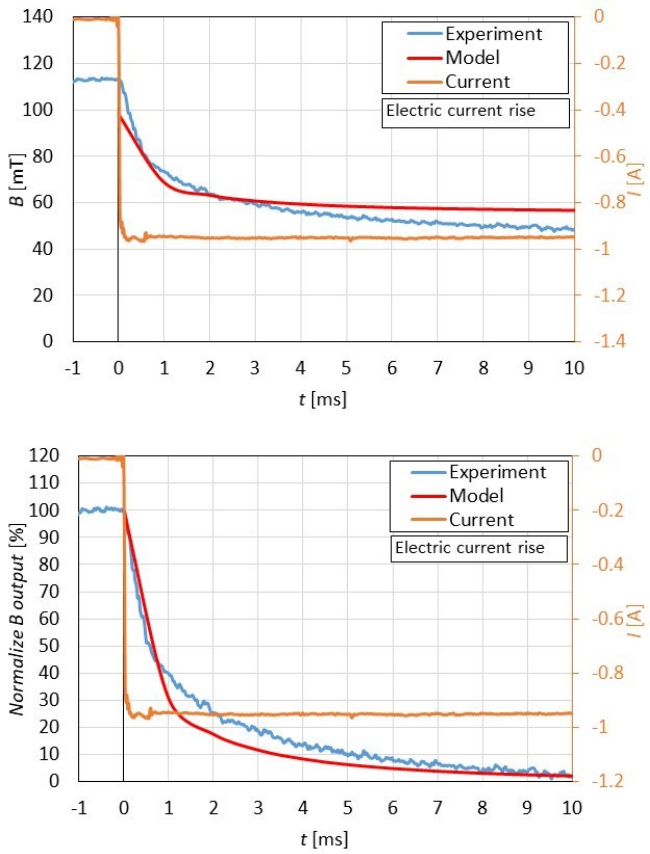

Figure 14 *The course of magnetic flux density from the magnetic model and experiment*

The difference in magnetic flux density B course from the model and the experiment is probably due to the slightly different electrical conductivity of the material uses in the model. The electric conductivity was used from the datasheet of the steel suppliers. The initial and final magnetic flux density data from the model and experiment exhibits roughly 15 % difference, see **Figure 14**. This error is probably caused by the fitting of the hysteresis model to measured the hysteresis loop of magnetic circuit material, see **Figure 6**. The accuracy of the magnetic model is very good in the context of many possible materials (slightly different chemical composition of steel, a measurement error of B-H curve, etc.) inaccuracies. The primary and secondary response time dependency on the electric current are shown in **Figure 15**. All values presented in diagram labelled "rise" were measured for initial current in the coil I = 0A (fail-safe state). On the other hand, the data presented in diagram labelled "drop" were measured for final value of current I = 0A. The presented response time values in the next text sections (if are available) are always experimental data. The response time for the negative polarity (*-I*) of electric current is significantly lower than positive polarity (*+I*). The primary response time for the electric current *rise* from *0A* to *-2A* is $\tau_{63} = 0.95\ ms$ and for electric current *drop* from *-2A* to *0A* is $\tau_{36} = 0.97\ ms$. The primary response time for the electric current *rise* from *0A* to *2A* is $\tau_{63} = 4.6\ ms$ and for a *drop* from *2A* to *0A* is $\tau_{36} = 3.6\ ms$. The magnetic flux density decrease in the gap is significantly faster than the increase. The *magnet* significantly *influences* the *dynamic behavior of the magnetic circuit*. The magnetic model describes the primary response time very well. The secondary response time exhibits greater variance, especially for the electric current drop. The magnetic model can be considered experimentally verified.

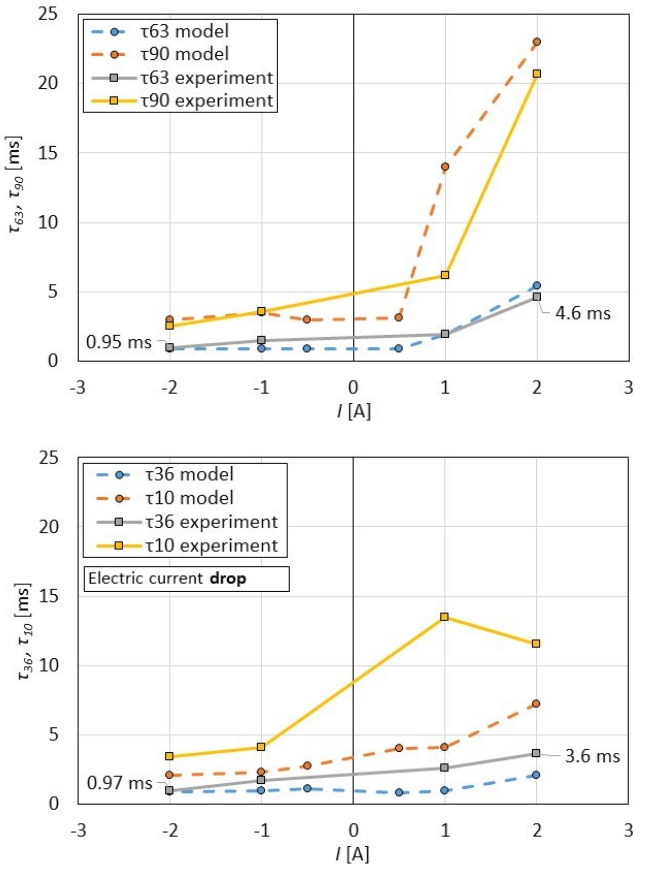

Figure 15 *The primary and secondary response time for configuration with air in the gap*

3.2.2 Magnetic circuit with MRF (coil)

The experimentally verified magnetic model was used to determine the dynamic behavior of the magnetic circuit with MRF in the gap (no magnet). The response time for the electric current drop and rise are presented in **Figure 16**. The response time dependency on electric current is non-linear. For electric current rise, the lower the electric current, the greater the response time. For electric current drop, the tendency is the opposite up to 0.5 A. Than the response time is stabilized. Thus, it can be stated that the *response time is dependent* on the final magnitude of the *electric current*. Similar results are published [31]. However, this dependence is probably related to the design of the magnetic circuit (geometry) and the

magnetization characteristics of the used material. These trends are supported by several simulations and publications.

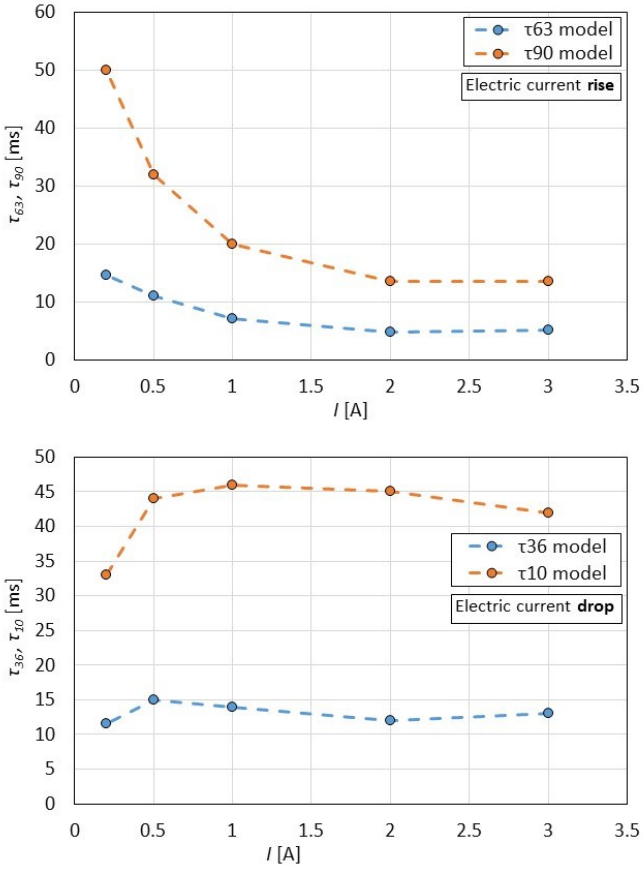

Figure 16 *The response time dependency of electric current for configuration with the coil (no magnet) and MRF*

3.2.3 Magnetic circuit with MRF (magnet and coil)

Figure 17 shows the dependence of the response time on step electric current drop and rise input. The response time for the current rise is increasing up to *0.5A*, then significantly decreases. The response time is τ_{63} = *17 ms* and τ_{90} = *53 ms* for the electric current rise from *0A* to *0.5A*. The trends are similar as in the case of configuration without magnet. In the opposite electric current polarity (*-I*), the primary and secondary time responses are almost independent of the magnitude of the electric current. The response time is τ_{63} = *1.1 ms* and τ_{90} = *5 ms* for electric current rise from *0A* to *-1A*. The drop of magnetic induction in the gap is *15 times* faster (primary response time) and *10 times* faster (secondary response time) than the rise. The magnetic circuit dynamic is almost independent of the rising or dropping of electric current in opposite electric current polarity (*-I*). However, the rise and drop for electric current have a different tendency for positive polarity. The response time is τ_{36} = *14.5 ms* and τ_{10} = *50 ms* for electric current drop from *1A* to *0A*. The response time is stabilized after achieved *1A*. It can be deduced that the short response time of magnetic field formation with the negative polarity of electric current is *not* related to MR fluid because this effect was observed also in the magnetic circuit without MRF, see **Figure 15**.

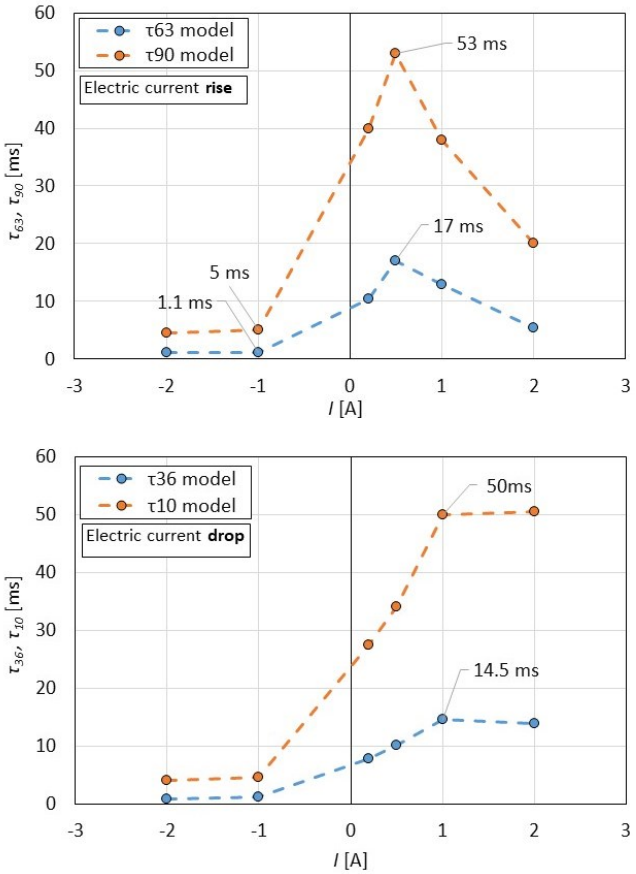

Figure 17 *The response time dependency of electric current for configuration with an electromagnetic coil, magnet, and MRF*

3.3 F-v-I map

Based on the methodology described in Chapter 2.4, the force-velocity (F-v) maps were measured for *2A, 1A, 0A (+), -1A, -2A* and *0A*(-) electric currents, see **Figure 18**. The F-v map for no electric current is affected by magnetization history (previous orientation of electric current). The damping force for zero electric current and change from higher damping forces (*+0A*) is higher than the switch from lower damping forces (*-0A*). The damping force for *+0A* was *592 N* and for *-0A* was *505 N* at piston velocity *0.1 m/s*. This is a *15%* decrease. This difference is due to the hysteresis behavior of the magnetic circuit itself, as described in **Figure 13**. The force *505 N* corresponds with magnetic induction *127 mT* and force *592 N* with magnetic induction *178 mT*. This difference could be reduced by using another material of magnetic circuit (SMC, Vacoflux, etc.) or by selecting a suitable heat treatment. Fail-safe damping force is approximately *1/3* of the maximum damping force (*0.1 m/s*).

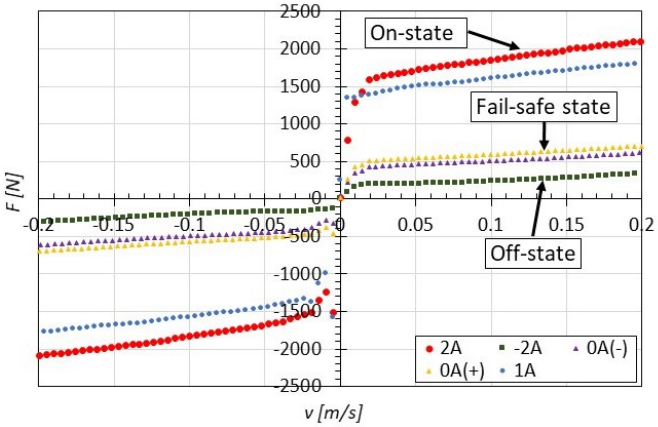

Figure 18 *Force-velocity map of fail-safe MR damper*

The dynamic force range of damper was calculated from the maximum (*+2A*) a minimum (*-2A*) damping forces at given piston velocity, see **Figure 19**. The maximum dynamic force range is *8.5* at the piston velocity of *0.06 m/s*. The presented fail-safe MR damper achieves a comparable dynamic force range as the non-permanent magnet MR damper variants [3,9,16]. The dynamic force range of the damper is also one of the essential parameters for efficient S/A control [6].

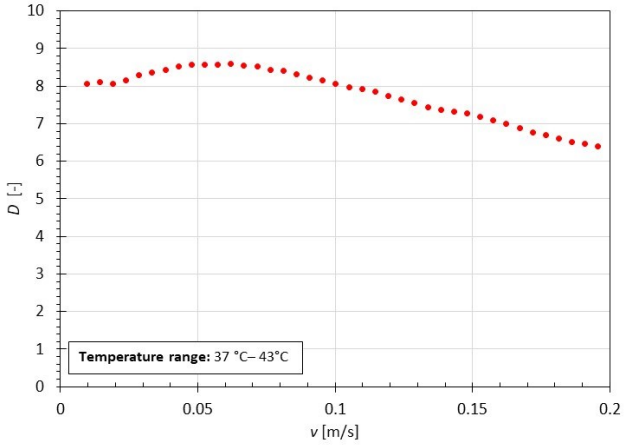

Figure 19 *Dynamic force range of MR damper with magnet*

3.4 MR damper dynamics (force response time)

The force courses on the step current input were measured according to the methodology described in chapter 2.5. **Figure 24** shows the course of force (blue) and electric current orange) for step current drop input from -2A to 0A at piston velocity 0.3 m/s. The measured force data was normalized, see **Figure 21**. In all the measured data, it can be seen the time delay approximately 0.5-0.8 ms between the course of electric current and force. This time delay was *not* observed in the course of magnetic induction, see **Figure 21**, which means that it must be related to the hydraulic system.

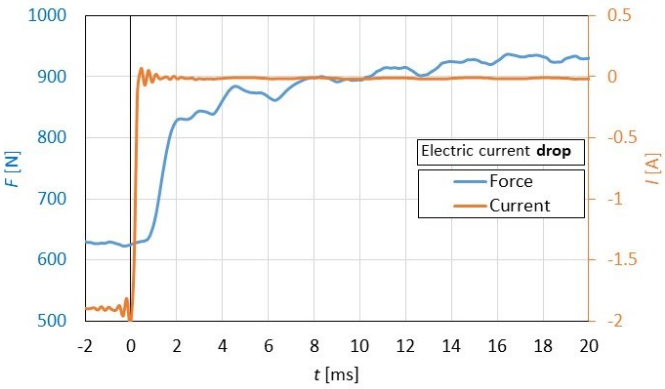

Figure 20 *example of the course of the force and electric current for unit-step electric current drop input at piston velocity 0.3 m/s.*

It was checked that this time delay is not due to measurement devices or their settings. This time delay is probably caused by the response time of MR fluid itself or deformation of the rubber part of the damper (seal). Similar conclusions have been published in [17]. This phenomenon will be detailed studied in the following research.

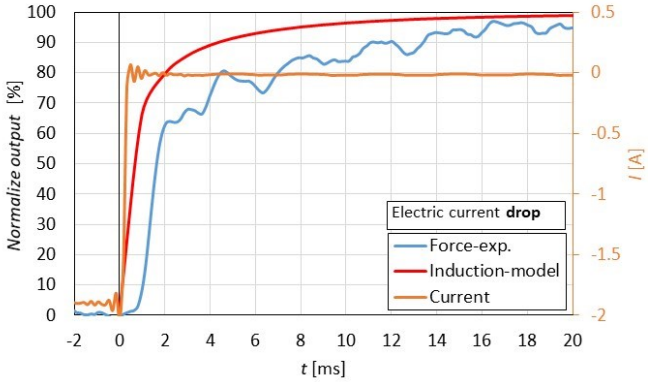

Figure 21 *Normalize course of force and magnetic induction*

The data from the magnetic model was moved of 0.8 ms due to the presented delay, see **Figure 22**. The magnetic model well describes the initial course of force.

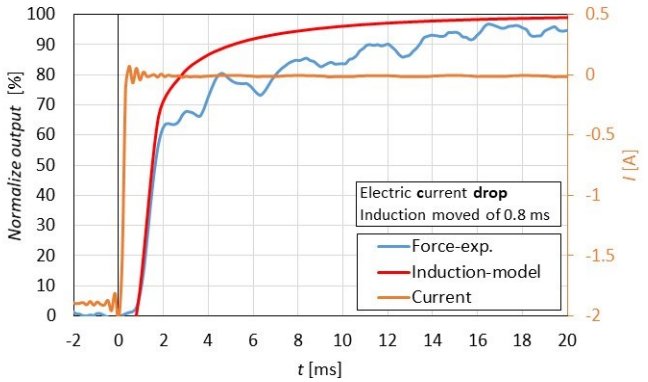

Figure 22 *Normalize course of force and magnetic induction (moved of 0.8 ms)*

The force course exhibits significant pulsation due to the hydraulic system compliance [9]. Therefore, the determination of secondary response time is quite inaccurate and exhibits a large dispersion. The comparison of response time dependency on electric current from force measurement and magnetic model is presented in **Figure 23** and **Figure 24**. The force measurement dispersion is presented by error bars that show maximum, minimum measured force value, and also average value.

Electric current step rise

The primary (τ_{63}) and secondary (τ_{90}) force response time is strongly dependent on electric current polarity and magnitude, see **Figure 23**.

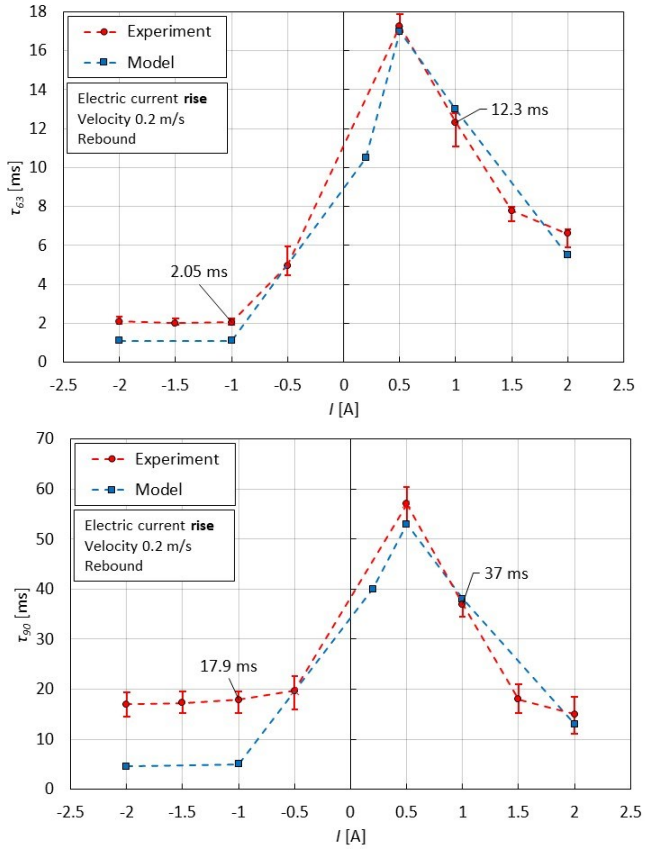

Figure 23 *The course of primary and secondary response time on orientation and magnitude of electric current for configuration with electric current step rise; force data (red circle), magnetic model data (blue square)*

The response time is significantly lower for the negative orientation of electric current (form *0A* to *-1A*; force data τ_{63} = *2.05 ms*, τ_{90} = *17.9 ms*) than for positive orientation (from *0A* to *1A*; force data τ_{63} = *12.3 ms*, τ_{90} = *37 ms*). The drop of force is app. 6 times faster than rising. The primary response time determined from the magnetic model well fit experimental data, see **Figure 23**. The secondary response time from the magnetic model also well fit experimental data except for the negative orientation of electric current. There is a significant difference.

Electric current step drop

The primary (τ_{63}) and secondary (τ_{90}) force response time is also strongly dependent on electric current orientation and magnitude, see **Figure 24**.

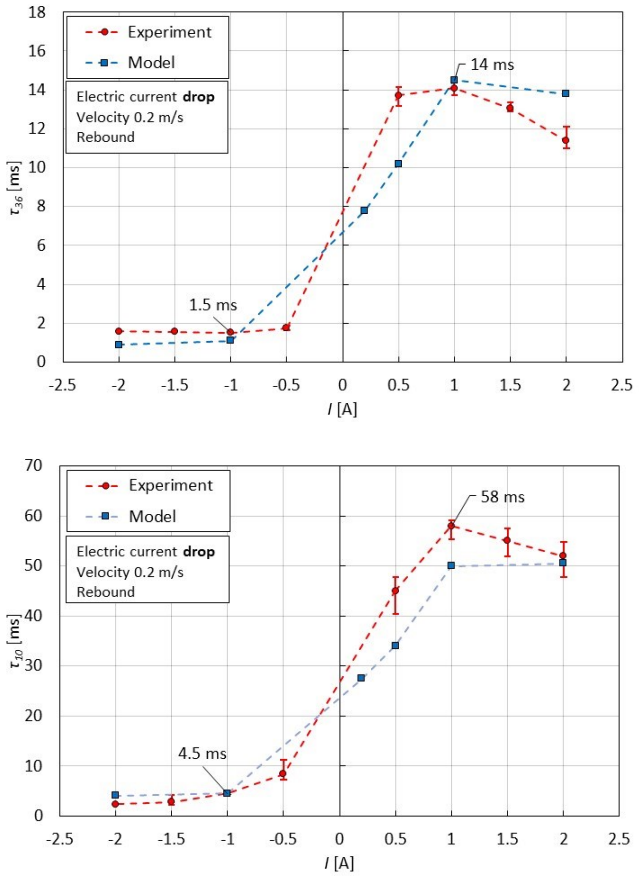

Figure 24 *The course of primary and secondary response time on orientation and magnitude of electric current for configuration with electric current step drop; force data (red circle), magnetic model data (blue square)*

It can be seen that negative orientation of electric current (from *-1A* to *0A*; τ_{36} = *1.5 ms*, τ_{10} = *4.5 ms*) is significantly faster than positive orientation (from *1A* to *0A*; τ_{36} = *14 ms*, τ_{10} = *58 ms*). In this case, the magnetic model very well fit experimental data. It should be noted that the presented data are connected with the exact geometry and material configuration of the MR valve. It can be assumed that the exact value of response time will be dependent on the specific geometry and material configuration of the MR valve. However, the trend will be the same.

Influence of piston velocity on force response time

Figure 25 shows the influence piston velocity on primary response time for the rise of the damping force. The primary

response time slightly increases at a piston velocity of *0.1* m/s. This increase is caused by the rigidity of the hydraulic system itself especially the rigidity of MR fluid. This phenomenon is also described in [9].

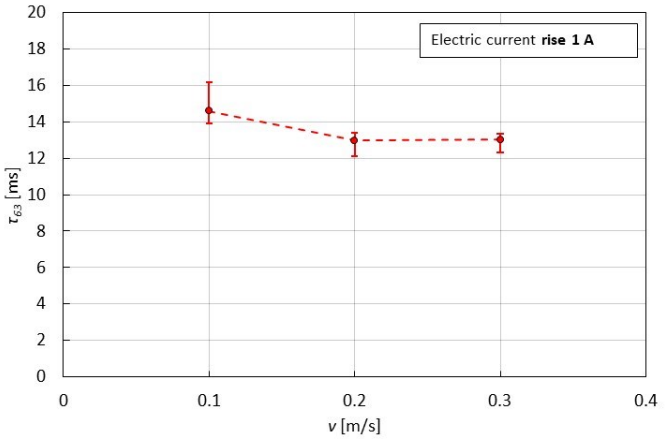

Figure 25 The influence of piston velocity on primary response time

4. Conclusion

The optimal performance of a semi-active suspension system with fail-safe MR damper requires understanding its dynamic behavior. The knowledge of time delay between force and control signal is necessary for accurate control design study or vehicle dynamic simulations. This paper presented the dynamic behavior of MR damper with the permanent magnet. The conclusions from this paper are the following:

- The magnetic flux density in the gap at zero electric current creates roughly 1/4 of maximum and is magnetization history dependent due to hysteresis behaviour of magnetic circuit material.
- The magnetic flux density in the gap decreases significantly faster than increases on the electric current step. This is probably given by the effect of permanent magnet.
- The fail-safe damping force at zero electric current is also dependent on magnetization history and the achieved app. 1/3 of maximum damping force. The difference at fail-safe forces is due to the hysteresis behavior of the magnetic circuit.
- The dynamic force range of fail-safe MR damper achieved a value of *8.5* which similar to the common design of MR damper. The maximum damping forces are also comparable.
- The *decrease* in the *damping force* (negative polarity of electric current) from a fail-safe state to off-state is significantly faster than the increase from fail-safe state to on-state. The primary response time is roughly *2 ms*. This short response time in probably given by the effect of the permanent magnet.
- The *increase* in the *damping force* (positive polarity of electric current) from fail-safe state to on-state is significantly slower than the decrease and strongly dependent on the magnitude of the electric current. The primary response time achieved roughly *12 ms* at electric current *1A*.
- The initial time delay of *0.5* - *0.8* ms between the course of force and an electric current was observed. This delay wasn't observed in magnetic flux density measurement. Therefore, this delay is probably caused by hydraulic system compliance or response time MR fluid itself.
- The response time determined from the magnetic model well fitted experimental force data of MR damper. For this reason, a transient magnetic simulation is an effective tool for the determination of the dynamic behaviour of MR damper.

The following research will be focused on the durability of this type of damper and fail-safe behaviour dependency on temperature.

Acknowledgement

The authors wish to acknowledge the support of the grant FEKT/FSI-J-20-6260, GAČR 20-23261Y and FSI-S-20-6247.

References

[1] Westerhoff M 2018 ZF Vision magazine
[2] Karnopp D, Crosby M J and Harwood R A 1973 Vibration Control Using Semi-Active Force Generators. *ASME Pap* 619–26
[3] Strecker Z, Mazůrek I, Roupec J and Klapka M 2015 Influence of MR damper response time on semiactive suspension control efficiency *Meccanica* **50** 1949–59
[4] Koo J H, Goncalves F D and Ahmadian M 2006 A comprehensive analysis of the response time of MR dampers *Smart Mater. Struct.* **15** 351–8
[5] Giua A, Melas M and Seatzu C 2004 Design of a control law for a semiactive suspension system using a solenoid valve damper *Proc. IEEE Int. Conf. Control Appl.* **2** 1467–72
[6] Machacek O, Kubik M and Novák P 2017 A new method of magnetorheological damper quality evaluation *Eng. Mech. 2017* 594–7
[7] Qin Y, Zhao F, Wang Z, Gu L and Dong M 2017 Comprehensive analysis for influence of controllable damper time delay on semi-active suspension control strategies *J. Vib. Acoust. Trans. ASME* **139**
[8] Li P X, Su M and Zhang D B 2017 Response characteristic of high-speed on/off valve with double voltage driving circuit *IOP Conf. Ser. Mater. Sci. Eng.* **220**
[9] Kubík M and Goldasz J 2019 Multiphysics Model of an MR Damper including Magnetic Hysteresis *Shock Vib.* **2019**
[10] Roupec J, Berka P, Mazůrek I, Strecker Z, Kubík M, Macháček O and Andani M T 2017 A novel method for measurement of MR fluid sedimentation and its experimental verification *Smart Mater. Struct.* **26** 107001
[11] Cheng H, Wang M, Liu C and Wereley N M 2018 Improving sedimentation stability of magnetorheological fluids using an organic molecular particle coating *Smart Mater. Struct.* **27**
[12] Plachy T, Cvek M, Kozakova Z, Sedlacik M and Moucka R 2017 The enhanced MR performance of dimorphic MR suspensions

containing either magnetic rods or their non-magnetic analogs *Smart Mater. Struct.* **26**

[13] Cvek M, Mrlik M, Ilcikova M, Plachy T, Sedlacik M, Mosnacek J and Pavlinek V 2015 A facile controllable coating of carbonyl iron particles with poly(glycidyl methacrylate): A tool for adjusting MR response and stability properties *J. Mater. Chem. C* **3** 4646–56

[14] Zheng J, Li Y and Wang J 2017 Design and multi-physics optimization of a novel magnetorheological damper with a variable resistance gap *Proc. Inst. Mech. Eng. Part C J. Mech. Eng. Sci.* **231** 3152–68

[15] Gołdasz J 2013 Electro-mechanical analysis of a magnetorheological damper with electrical steel laminations *Prz. Elektrotechniczny* **89** 8–12

[16] Kubík M, Macháček O, Strecker Z, Roupec J and Mazůrek I 2017 Design and testing of magnetorheological valve with fast force response time and great dynamic force range *Smart Mater. Struct.* **26** 1–9

[17] Strecker Z, Kubik M, Vitek P, Roupec J, Paloušek D and Šreibr V 2019 Structured magnetic circuit for magnetorheological damper made by selective laser melting technology *Smart Mater. Struct.* **28**

[18] Goldasz J 2019 Magnetostatic study of a dual-gap MR valve *Proc. 2019 20th Int. Conf. Res. Educ. Mechatronics, REM 2019* **5** 1–5

[19] Goldasz J 2013 Study of a magnetorheological fl uid damper with multiple annular fl ow gaps *Int. J. Veh. Des.* **62** 21–41

[20] Bai X X and Wereley N M 2014 A fail-safe magnetorheological energy absorber for shock and vibration isolation *J. Appl. Phys.* **115** 1–4

[21] Zhang H H, Liao C R, Yu M and Huang S L 2007 A study of an inner bypass magneto-rheological damper with magnetic bias *Smart Mater. Struct.* **16** N40–6

[22] Yan W, Ji J, Dong B and Ge H 2009 Theoretical and experimental studies on a new reversible magnetorheological damper *Struct. Control Heal. Monit.* n/a-n/a

[23] Du C, Wan F and Yu G 2011 A magnetic flux leakage study of a self-decoupling magnetorheological damper *Smart Mater. Struct.* **20** 065019

[24] Böse H and Ehrlich J 2012 Magnetorheological dampers with various designs of hybrid magnetic circuits *J. Intell. Mater. Syst. Struct.* **23** 979–87

[25] Bose H, Ehrlich J and Trendler A-M 2009 Performance of magnetorheological fluids in a novel damper with excellent fail-safe behavior *11th Conference on Electrorheological Fluids and Magnetorheological Suspensions* p 5

[26] Takesue N, Kiyota Y and Furusho J Development of fast response MR-fluid actuator *Proceedings of the 41st SICE Annual Conference. SICE 2002.* vol 2 (Soc. Instrument & Control Eng. (SICE)) pp 949–53

[27] Strecker Z, Roupec J, Mazurek I, Machacek O, Kubik M and Klapka M 2015 Design of magnetorheological damper with short time response *J. Intell. Mater. Syst. Struct.* **26** 1951–8

[28] Kostamo E, Kostamo J, Kajaste J and Pietola M 2012 Magnetorheological valve in servo applications *J. Intell. Mater. Syst. Struct.* **23** 1001–10

[29] Sahin H, Gordaninejad F, Wang X and Liu Y 2012 Response time of magnetorheological fluids and magnetorheological valves under various flow conditions *J. Intell. Mater. Syst. Struct.* **23** 949–57

[30] Maas J and Güth D 2011 Experimental Investigation of the Transient Behavior of MR Fluids *Conference on Smart Materials, Adaptive Structures and Intelligent Systems* (ASME) pp 1–9

[31] Wu G, Feng Z, Gang Zhang and Hou Z 2011 Experimental study on response time of magnetorheological damper *International Conference on Artificial Intelligence, Management Science and Electronic Commerce* (IEEE) pp 3968–72

[32] Lee T-H and Choi S-B 2019 On the response time of a new permanent magnet based magnetorheological damper: experimental investigation *Smart Mater. Struct.* **28** 014001

[33] Yoon D S, Park Y J and Choi S B 2019 An eddy current effect on the response time of a magnetorheological damper: Analysis and experimental validation *Mech. Syst. Signal Process.* **127** 136–58